ON THE HYDRODYNAMIC INTERPLAY BETWEEN A YOUNG NUCLEAR STARBURST AND A CENTRAL SUPERMASSIVE BLACK HOLE

Filiberto Hueyotl-Zahuantitla[1], Guillermo Tenorio-Tagle[1,2,4], Richard Wünsch[3], Sergiy Silich[1], and Jan Palouš[3]

[1] Instituto Nacional de Astrofísica Optica y Electrónica, AP 51, 72000 Puebla, Mexico; silich@inaoep.mx

[2] Institute of Astronomy, University of Cambridge, Madingley Road, Cambridge CB3 0HA, UK

[3] Astronomical Institute, Academy of Sciences of the Czech Republic, Boční II 1401, 141 31 Prague, Czech Republic

ABSTRACT

We present one-dimensional numerical simulations, which consider the effects of radiative cooling and gravity on the hydrodynamics of the matter reinserted by stellar winds and supernovae within young nuclear starbursts (NSBs) with a central supermassive black hole (SMBH). The simulations confirm our previous semi-analytic results for low-energetic starbursts, evolving in a quasi-adiabatic regime, and extend them to more powerful starbursts evolving in the catastrophic cooling regime. The simulations show a bimodal hydrodynamic solution in all cases. They present a quasi-stationary accretion flow onto the black hole, defined by the matter reinserted by massive stars within the stagnation volume and a stationary starburst wind, driven by the high thermal pressure acquired in the region between the stagnation and the starburst radii. In the catastrophic cooling regime, the stagnation radius rapidly approaches the surface of the starburst region, as one considers more massive starbursts. This leads to larger accretion rates onto the SMBH and concurrently to powerful winds able to inhibit interstellar matter from approaching the NSB. Our self-consistent model thus establishes a direct physical link between the SMBH accretion rate and the nuclear star formation activity of the host galaxy and provides a good upper limit to the accretion rate onto the central black hole.

Key words: accretion, accretion disks – galaxies: active – galaxies: starburst – hydrodynamics

1. INTRODUCTION

Powerful starbursts have been conclusively detected in the nuclear regions of galaxies with active galactic nuclei (AGNs; see, for a review, Veilleux et al. 2005; Heckman 2009). These include quasars (Hao et al. 2005, 2008), Seyferts (Imanishi 2003; Davies et al. 2007; Watabe et al. 2008; Chen et al. 2009), submillimeter galaxies with an extreme star formation rate (Alexander et al. 2005; Walter et al. 2009), and even low-luminosity AGNs (Cid Fernandes & Terlevich 1995; González-Delgado et al. 2004). Some supermassive black holes (SMBHs) coincide with massive and compact nuclear star clusters (Seth et al. 2008); some of them with a complex history of star formation are found in a number of nearby spiral (Rossa et al. 2006) and elliptical galaxies (Wehner & Harris 2006; Côté et al. 2006).

The interplay between young nuclear starbursts (NSBs) and their central SMBHs is not well understood and remains one of the central issues in the theory of AGN galaxies, and in the process of cosmological growth of SMBHs (Lípari & Terlevich 2006; Booth & Schaye 2009) and their co-evolution with the bulges of their host galaxies (Begelman & Nath 2005; Di Matteo et al. 2005; Somerville et al. 2008). In fact, even basic issues regarding, for example, the impact of Type II supernovae (SNe) on the matter left over from star formation, seem to be still undecided. One can find in the literature massive starbursts with an SN rate of 1 yr^{-1} structuring a gaseous disk of just $10^7 M_\odot$ (Wada & Norman 2002) while other calculations assume that Type II SN might evacuate most of the nuclear region from gas and dust (Schartmann et al. 2009) and have considered only the evolution after the end of the Type II SN epoch.

Silich et al. (2008) presented a self-consistent, spherically symmetric stationary solution for the gaseous flow around an SMBH at the center of a young ($\leqslant 40$ Myr) starburst region.

They also found a threshold mechanical luminosity (L_{crit}) which separates systems evolving in the quasi-adiabatic regime with a small stagnation radius, R_{st} (at which the velocity is 0 km s^{-1}) and consequently a low accretion rate, from those with a large R_{st} and a high accretion rate whose hydrodynamics are strongly affected by radiative cooling (see their Figure 6). The self-consistent semi-analytic solution found by Silich et al. (2008) is only valid for NSBs with a mechanical luminosity $L_{NSB} < L_{crit}$. Above the threshold luminosity, strong radiative cooling drives the gas thermally unstable. This has a strong impact on the thermal pressure gradient and thus on the location of the stagnation radius, facts which inhibit a complete semi-analytic solution. Thus, cases with a mechanical luminosity $L_{NSB} > L_{crit}$ demand a numerical integration of the flow equations. Nevertheless, from the semi-analytic results of Silich et al. (2008) it was suggested that the thermalization of the kinetic energy released within the volume occupied by a young NSB should lead to a central well-regulated accretion flow onto the massive object, while a powerful wind, capable of preventing the accretion of the ambient interstellar gas (interstellar medium (ISM)) onto the SMBH, should emanate from the outer regions. Here, we follow these suggestions and measure the power of the resultant winds, as well as the accretion rates onto the SMBH and show how their luminosity correlates with the starburst parameters. Following Nulsen & Fabian (2000) and Ciotti et al. (2009), we have assumed that the angular momentum of the thermalized gas is not too large and here we present results from our one-dimensional (1D) numerical simulations as a first approximation. The simulations confirm the semi-analytic results of Silich et al. (2008) and extend them to starbursts with a mechanical energy input rate, $L_{NSB} > L_{crit}$. In this paper, the input physics account for the mechanical feedback that a young NSB may provide the accretion flow while allowing for radiative cooling and the gravitational pull from both the central SMBH and the NSB. The feedback provided by the central SMBH (Silk & Rees 1998; Ciotti & Ostriker

---

[4] Sackler Visiting Fellow.

2001; Ciotti et al. 2009) will be the subject of a forthcoming communication.

The paper is organized as follows: the numerical scheme used and the initial and boundary conditions are presented in Section 2. Section 3 deals with the results from the simulations and compares them with the semi-analytic results. In Section 4, the accretion rates and luminosities of the central SMBHs are obtained, together with a measure of the possible impact of the resultant winds onto the host galaxy ISM. Section 5 gives our conclusions.

2. NUMERICAL APPROACH

The numerical model is based on the finite difference Eulerian hydrodynamic code ZEUS3D v.3.4.2, which solves the set of the hydrodynamic equations (Stone & Norman 1992; Wünsch et al. 2008):

$$\partial\rho/\partial t + \nabla \cdot (\rho u) = q_m, \tag{1}$$

$$\partial u/\partial t + (u \cdot \nabla)u + \nabla P/\rho = -\nabla\phi_{\mathrm{BH+NSB}}, \tag{2}$$

$$\partial e/\partial t + \nabla \cdot (eu) + P\nabla u = q_e - Q, \tag{3}$$

where q_m and q_e are the mass and energy deposition rates per unit volume, e is the internal energy, $Q = n_i n_e \Lambda(T, Z)$ is the cooling rate, n_i and n_e are the ion and electron number densities, and $\Lambda(T, Z)$ is the cooling function, which depends on the thermalized gas temperature, T, and metallicity, Z. The Raymond & Cox cooling function tabulated by Plewa (1995) has been used in all calculations. The right-hand side of Equation (2) represents the gravitational acceleration $a_g = -GM_r/r^2$, where $M_r = M_{\mathrm{BH}} + M_{\mathrm{NSB}}(r/R_{\mathrm{NSB}})^3$ is the mass within a volume of radius r. Outside of the starburst volume, $r > R_{\mathrm{NSB}}$, it is $M_r = M_{\mathrm{BH}} + M_{\mathrm{NSB}}$.

All simulations have been carried out in spherical coordinates with symmetry along the θ- and ϕ-directions and with a uniform grid in the radial direction. The calculations account for fast radiative cooling (see Tenorio-Tagle et al. 2007; Wünsch et al. 2008) and include the gravitational pull from the central SMBH and from the starburst, assuming that the stars are homogeneously distributed within a spherically symmetric volume.

2.1. Initial and Boundary Conditions

The initial distributions of velocity, pressure, temperature, and density for all calculations were taken from the semi-analytic wind solution (Silich et al. 2004), without accounting for the gravitational pull from the starburst and the central SMBH. The initial condition is adapted to starbursts of the required size (see Table 1), with a mechanical luminosity $L_{\mathrm{NSB}} < L_{\mathrm{crit}}$. The mechanical luminosity $L_{\mathrm{NSB}} = \dot{M}_{\mathrm{NSB}} V_{A,\infty}^2/2$, (where, $V_{A,\infty}$ is the adiabatic outflow terminal speed, assumed to be 1500 km s^{-1} in all calculations) has been normalized to the average mechanical luminosity for instantaneous starbursts with a Salpeter initial mass function, sources between $1\,M_\odot$ and $100\,M_\odot$, and with ages less than 10 Myr, $L_{\mathrm{NSB}} = 3 \times 10^{40}(M_{\mathrm{NSB}}/10^6\,M_\odot)$ erg s^{-1} (Leitherer et al. 1999). The reinserted gas was assumed to have a negligible angular momentum and thus the flow could be solved in spherical symmetry.

The mass and energy deposition rates per unit volume are $q_m = 3\dot{M}_{\mathrm{NSB}}/4\pi R_{\mathrm{NSB}}^3$ and $q_e = 3L_{\mathrm{NSB}}/4\pi R_{\mathrm{NSB}}^3$, respectively, where $\dot{M}_{\mathrm{NSB}}$ is the total mass deposition rate within the starburst

Table 1
Input Models

| Model	R_{NSB} (pc)	M_{NSB} ($10^8\,M_\odot$)	$\log(L_{\mathrm{NSB}})$	$L_{\mathrm{NSB}}/L_{\mathrm{crit}}$	$\dot{M}_{\mathrm{NSB}}$ ($M_\odot$ yr^{-1})
(1)	(2)	(3)	(4)	(5)	(6)
1a	40	2.0	42.778	0.5	8.45
1b	40	4.0	43.079	1.0	16.89
1c	40	6.0	43.255	1.5	25.34
1d	40	6.8	43.302	1.7	28.72
1e	40	8.0	43.380	2.0	33.79
2a	10	0.3	41.954	0.27	1.27
2b	10	0.5	42.176	0.45	2.11
2c	10	1.0	42.477	0.9	4.22
2d	10	1.67	42.698	1.5	7.03
2e	10	2.22	42.823	2.0	9.38
2f	10	2.75	42.916	2.5	11.61
2g	10	10.0	43.477	9.0	42.23
2h	10	20.0	43.778	18.0	84.46

Notes. The starburst input parameters for the simulations. Column 1 is a reference to the models. The radius (R_{NSB}), mass (M_{NSB}), logarithm of mechanical power (L_{NSB}, measured in erg s^{-1}), the ratio of the starburst mechanical power to the critical mechanical luminosity ($L_{\mathrm{NSB}}/L_{\mathrm{crit}}$), and the total starburst mass deposition rate ($\dot{M}_{\mathrm{NSB}}$) are presented in Columns 2–6, respectively. All starburst models have a central SMBH with a mass $M_{\mathrm{BH}} = 10^8\,M_\odot$.

volume (see Table 1). These values are added, at each time step, to the computed density and total energy in every cell, ρ_{old} and $e_{\mathrm{tot,old}}$, respectively, when located inside the starburst volume using the following procedure: $\rho_{\mathrm{new}} = \rho_{\mathrm{old}} + q_m dt$, and the velocity is corrected so that the momentum is conserved, $v_{\mathrm{mid}} = v_{\mathrm{old}}\rho_{\mathrm{old}}/\rho_{\mathrm{new}}$, the internal energy is corrected to conserve the total energy, $e_{i,\mathrm{mid}} = e_{\mathrm{tot,old}} - \rho_{\mathrm{new}}v_{\mathrm{mid}}^2/2$, and the new energy is inserted as a form of internal energy $e_{i,\mathrm{new}} = e_{i,\mathrm{mid}} + q_e dt$ (see Tenorio-Tagle et al. 2007; Wünsch et al. 2008). The velocity of the flow at each radius is updated according to $v_{\mathrm{new}} = v_{\mathrm{mid}} + a_g dt$, where a_g is the gravitational acceleration at each radius (see Section 2). The computational domain extends over the interval ($R_{\mathrm{in}}, R_{\mathrm{out}}$), where $0 < R_{\mathrm{in}} \ll R_{\mathrm{NSB}} < R_{\mathrm{out}}$. An open boundary condition was adopted at both ends of the computational grid.

Our reference models are presented in Table 1. Here Column 1 is a reference to the model, while Columns 2–4 present the radius, mass, and mechanical luminosity of the considered starburst, respectively. The ratio of the starburst mechanical luminosity to the critical luminosity and the total mass deposition rate inside the starburst volume are shown in Columns 5 and 6. The mass of the central SMBH, unless explicitly mentioned, was assumed to be $M_{\mathrm{BH}} = 10^8\,M_\odot$ in all calculations. The computational domain for models 1a–e extends radially from $R_{\mathrm{in}} = 0.1$ pc to $R_{\mathrm{out}} = 50$ pc. The inner and outer radii of the computational domain in the case of models 2a–2h are 0.05 and 20 pc, respectively. One thousand grid zones were used in all calculations. The resolution convergency was tested in the case of the most energetic model (2h), carried out with 1000 and 3000 grid cells resolution. The results with both resolutions are in excellent agreement over the whole computational domain.

3. RESULTS

The results of the simulations are summarized in Table 2. Where Column 1 is a reference to the model, Column 2 presents the resultant stagnation radius. The total mass deposition rate
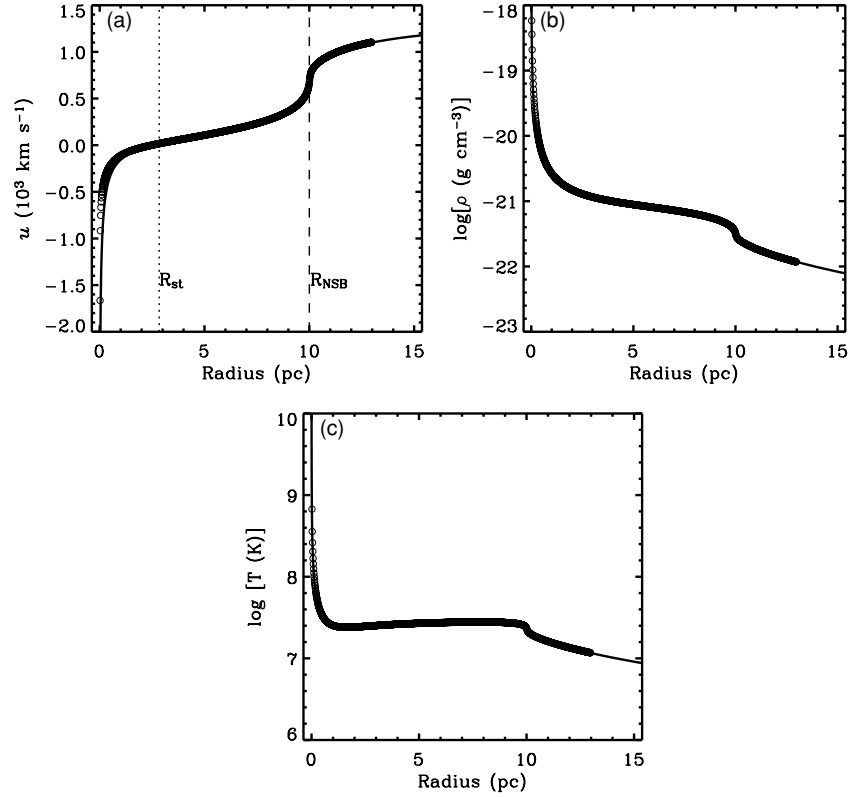
Figure 1. Test calculations. The numerical hydrodynamic solution (circles) for model 2c (see Table 2) is compared with the semi-analytic results (solid lines). Panels (a)–(c) show the run of the stationary velocity, density, and temperature across the radial direction. In panel (a), the dotted and dashed vertical lines mark the location of the stagnation radius and the nuclear starbursts radius, respectively.

Table 2
Predicted Accretion Rate and the Power of the Wind

Model	R_{st} (pc)	$\dot{M}_{NSB}$	$\dot{M}_{acc}$ ($M_\odot$ yr^{-1})	$\dot{M}_w$	L_{acc}/L_{Edd}	P_{ram} (10^{-7} dyn cm^{-2})
(1)	(2)	(3)	(4)	(5)	(6)	(7)
1a	2.1	8.45	1.88×10^{-3}	8.44	8.2×10^{-4}	1.96
1b	4.7	16.89	4.33×10^{-2}	16.86	1.9×10^{-2}	3.82
1c	11.4	25.34	0.93	24.72	0.4	5.39
1d	14.4	28.72	1.38	27.33	0.6	5.89
1e*	17.5	33.79	2.88	30.89	1.2	6.57
2a	1.3	1.27	5.09×10^{-3}	1.26	2.2×10^{-3}	4.66
2b	1.7	2.11	1.02×10^{-2}	2.07	4.5×10^{-3}	7.67
2c	2.8	4.22	0.14	4.09	6.1×10^{-2}	14.64
2d	4.4	7.03	0.59	6.45	2.6×10^{-1}	22.07
2e	5.3	9.38	1.36	8.00	0.6	26.83
2f*	5.9	11.61	2.38	9.23	1.04	30.53
2g*	8.2	42.23	23.28	18.74	10.2	56.16
2h*	8.9	84.46	59.54	25.48	26.0	77.43

Notes. The predicted accretion rate and the power of the wind. Column 1 is a reference to the models. The results of the calculations, the value of the stagnation radius (R_{st}), total starburst mass deposition rate ($\dot{M}_{NSB}$), the calculated mass accretion rate ($\dot{M}_{acc}$), the rate at which matter flows away from the starburst as a super wind ($\dot{M}_w$), the stationary SMBH accretion luminosity normalized to the Eddington limit (L_{acc}/L_{Edd}), and the ram pressure of the wind (P_{ram}) are shown in Columns 2–7, respectively. Asterisks mark those models for which the calculated accretion luminosity exceeds the Eddington limit.
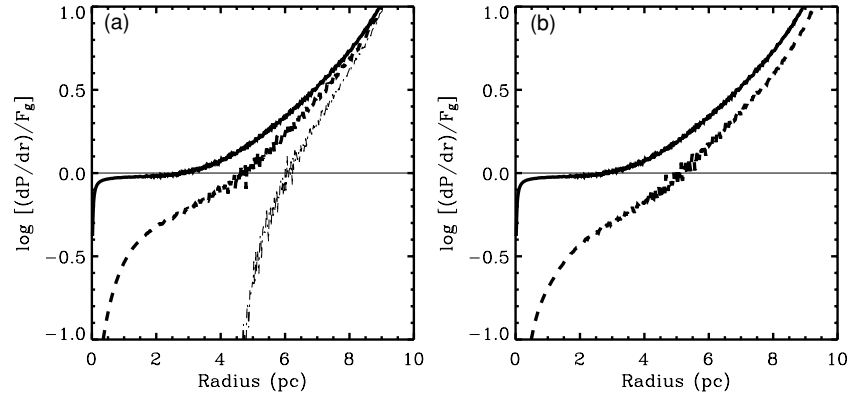
the outflow at the starburst edge ($P_{ram} = \rho u^2$) is presented in Column 7.

3.1. Comparison of the Numerical and the Semi-analytic Solutions

In order to test our numerical code, several simulations were carried out for starbursts with $L_{NSB} < L_{crit}$ to compare them with the semi-analytic model of Silich et al. (2008). Figure 1 presents, as an example, the results of the semi-analytic (solid line) and numerical (open circles) calculations for case 2c in Table 1. There is a good agreement between the two methods, as shown in panels (a)–(c), for the stationary run of velocity, density, and temperature, respectively. The value of the stagnation radius, marked by the dotted line in panel (a), is $R_{st} = 2.8$ pc, only about ~1.5% less than the value predicted by the semi-analytic model. The stationary solution shows how the matter deposited by massive stars inside the stagnation volume ends up falling toward the center and fuels the SMBH. On the other hand, matter reinserted between the stagnation radius and the starburst edge is steadily accelerated to reach its sound velocity at the starburst edge and then it expands supersonically forming the starburst wind. Note that as matter falls to the center, its density grows orders of magnitude due to convergency alone (panel (b)). The temperature also increases very sharply (panel (c)) due to the violent compression induced by the rapidly infalling matter.

3.2. The Numerical Solution Above the Threshold Line

The hydrodynamic solution for the matter reinserted by massive stars within an evolving young massive starburst in the presence of a central SMBH is always bimodal, whether

is shown in Column 3 and should be compared with the resultant accretion rate and the mass outflow in the starburst wind, presented in Columns 4 and 5, respectively. Column 6 shows the SMBH luminosity normalized to the Eddington limit ($L_{Edd} = 1.3 \times 10^{38} M_{BH} M_\odot^{-1}$ erg s^{-1}). The ram pressure of

Figure 2. Comparison of the pressure gradient to the gravity force inside the starburst volume. Panel (a) shows the ratio of the pressure gradient to the gravity force for starbursts of the same mass and radius (model 2c) but with different gas metallicities. Here, solid, dashed, and dotted lines correspond to $Z = Z_\odot$, $Z = 5\,Z_\odot$, and $Z = 10\,Z_\odot$, respectively. The intersection of the curves with the thin horizontal lines marks the position of the stagnation radius. The stagnation radius moves to a larger distance from the center as the cooling rate becomes larger. Panel (b) shows the same ratio for starbursts with different energy deposition rates (or different masses) but the same (solar) metallicity; the solid and dashed lines correspond to models 2c and 2e in Table 2, respectively.

one considers starbursts below or above the threshold line. The main difference is that above the threshold line strong radiative cooling becomes the physical agent that defines where the stagnation radius lies. The stationary location of the stagnation radius is defined by the balance between the gravitational force (F_g) and the outward thermal pressure gradient (dP/dr), which, naturally, is strongly affected by energy losses. Figure 2 presents the ratio of the pressure gradient to the gravity force as a function of distance from the center of the starburst. At the stagnation radius, $dP/dr = F_g$ and thus the intersection of lines which display this ratio with the thin horizontal line marks the position of the stagnation radius for various cases. Figure 2(a) shows the ratio of the pressure gradient to the gravity force for starbursts with identical mass and radii (equal to those of model 2c in Table 1) when the thermalized gas was assumed to have different metallicities. In these cases, the displacement of the stagnation radius to larger and larger values is promoted by the increasingly larger amount of energy lost through radiative cooling within the considered starburst. Similarly, radiative cooling is enhanced as one considers more massive starbursts. These reinsert more material per unit time and thus lead to a more significant radiative cooling, as shown in Figure 2(b), for cases 2c and 2e. In the region $r < R_{st}$, the outward pressure gradient is not able to compensate the gravity force and then all matter reinserted within the stagnation volume falls toward the central SMBH. On the other hand, in the region $R_{st} < r < R_{NSB}$ the pressure gradient exceeds the gravity force and hence the matter deposited there accelerates outward and conforms a supersonic wind. Similar trends were noticed in the 3D results from Schartmann et al. (2009) when considering the mass and energy input rate from planetary nebulae and Type I SNe in evolved clusters surrounding an SMBH. Here, however, we conclude that the amount of matter which fuels the central SMBH and that which forms the starburst wind, both depend directly on the location of the stagnation radius.

Figure 3 shows the results of numerical simulations for starbursts with a mechanical luminosity larger than L_{crit} (models 2e, 2g, and 2h). Here the upper, middle, and lower panels present the quasi-stationary distribution of the flow velocity, density, and temperature, respectively. As one considers more energetic (or more massive) starbursts, the larger densities (see middle panels) promote a faster radiative cooling within the thermalized plasma, and this results in a smaller pressure gradient and thus

in a further displacement of the stagnation radius toward larger distances from the starburst center. This is shown by vertical dotted lines in the upper panels.

The structure of the accretion flow for starbursts above the critical line presents some distinct features. In particular, the temperature distribution is different from that in the case of starbursts below the threshold line. It drops smoothly within the starburst region until a thermal instability develops within the accretion flow. The temperature then suddenly drops to the minimum permitted value as shown in the bottom panels of Figure 3.

Faster cooling also leads to a smaller wind speed. If one measures at a distance $r = 2R_{NSB}$ it is 1136 km s^{-1} in the less energetic considered case (model 2e) and 629 km s^{-1} in the most energetic case (model 2h), instead of the 1500 km s^{-1} expected in the adiabatic case. Note that for the most energetic case (model 2h), the temperature also drops suddenly to 10^4 K in the free-wind region.

Note that despite the continuous input of energy, the gas temperature remains then at the same value all the way, as it falls toward the center. Note also that the thermal instability appears at larger distances from the center as one considers a larger mass deposition rate or more massive and luminous starbursts (Figure 3, bottom panels). However, in all cases, the cold and supersonically infalling flow is well restricted to the central regions of the starburst, well within the stagnation volume. This is most probably the reason why the semi-analytic method is able to find with great accuracy the location of the stagnation radius, even for starbursts above the threshold line. Figure 4 presents the Jeans radius, $R_J = 0.5c_s(\pi/G\rho)^{1/2}$ (Clarke & Carswell 2007), where c_s is the local sound speed calculated at each r inside the stagnation volume for our most massive models 2g and 2h. In both cases, R_J would be larger than r if the central SMBH is able to photoionize the accretion flow, and the gas temperature cannot drop below 10^4 K. However, R_J may be smaller than r, and thus the accretion flow may become gravitationally unstable if the temperature falls below 10^3 K (Wada et al. 2009). Note, however, that for a given luminosity, the location of the stagnation radius is independent of the minimum temperature allowed in the flow, and therefore $\dot{M}_{acc}$ does not depend on the value of T_{min}, unless one quantifies star formation in the accretion flow, which is beyond the scope of the present study. Thus, the accretion flow is always gravitationally stable in the quasi-adiabatic regime, below the threshold line,
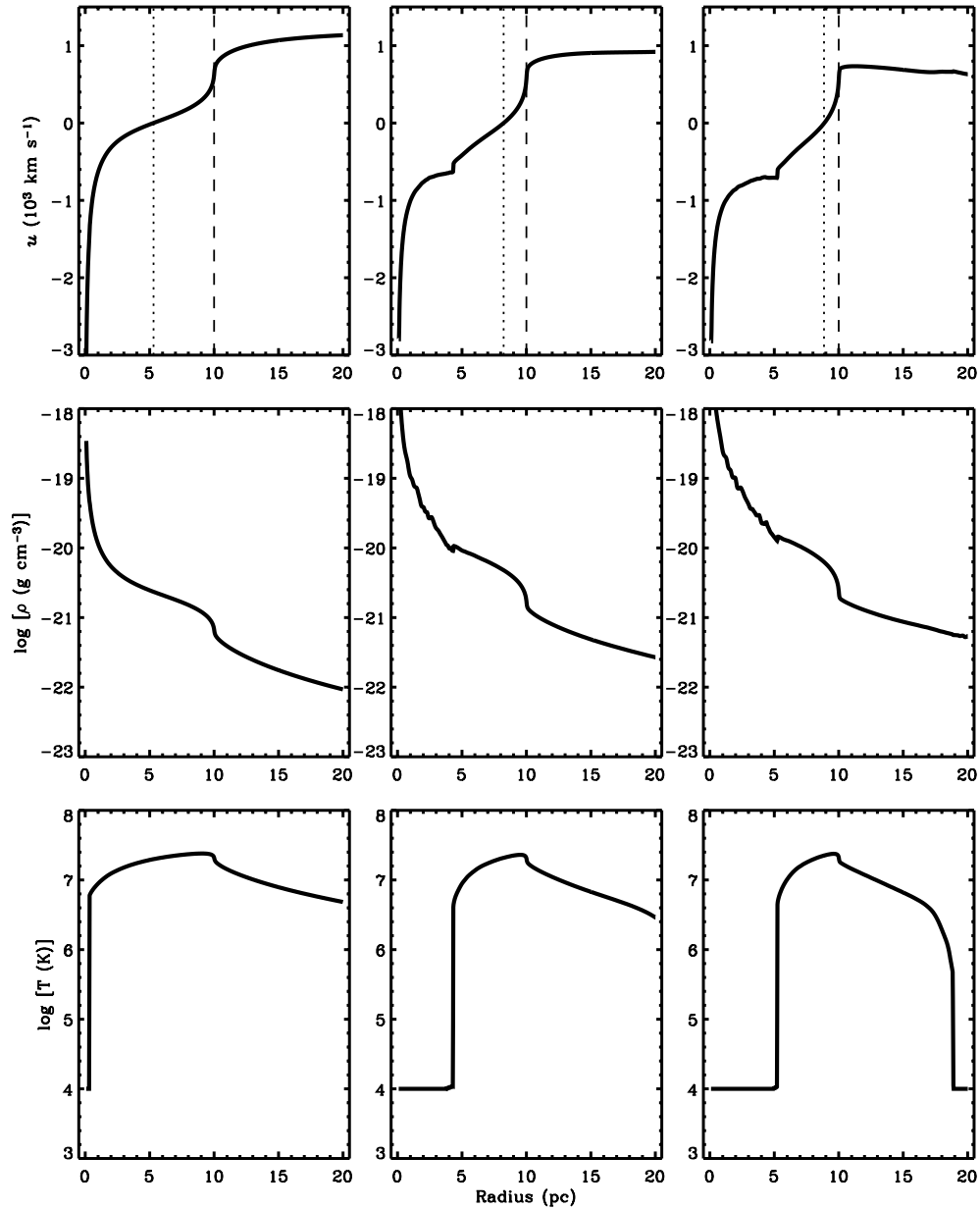
Figure 3. Hydrodynamic solution for starbursts with a mechanical luminosity $L_{NSB} > L_{crit}$ and a central SMBH. Panels from left to the right correspond to models 2e, 2g, and 2h, respectively. Upper, middle, and lower panels display the stationary velocity, density, and temperature distributions, respectively. Dotted and dashed lines in the upper panels mark the location of the stagnation and the starburst radii, respectively. The stagnation radius appears further out for more energetic (and thus more massive) starbursts, because the strong radiative cooling rapidly depletes the temperature to the minimum allowed in the calculations, $T_{min} = 10^4$ K, and this results in a sudden loss of pressure. The radius of the thermally unstable zone also grows as the mechanical power of the considered starburst increases.
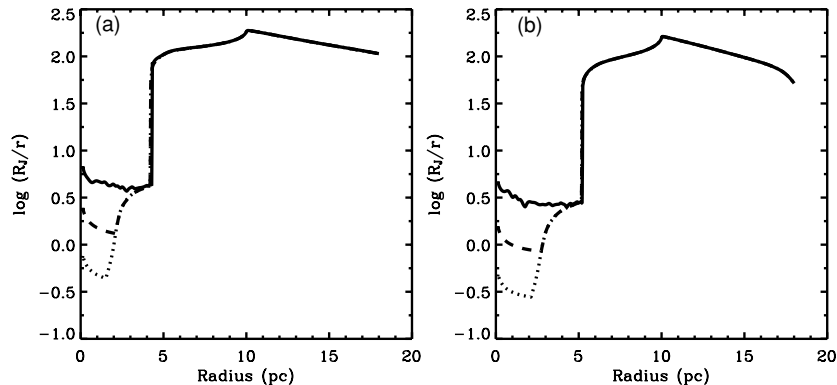
Figure 4. Ratio of the Jeans radius to the radius of the flow as a function of distance to the NSB center. Panels (a) and (b) present the results of the calculations for models 2g and 2h, respectively. The flow is gravitationally unstable if $R_J < r$. The solid, dashed, and dotted lines present $\log(R_J/r)$ for different minimum temperatures allowed in the calculations, $T_{min} = 10^4$, 10^3, and 10^2 K, respectively.

and becomes progressively more unstable above the critical line as one considers starbursts with a larger mechanical luminosity.

The reinserted matter thermalized inside the starburst region may contribute to the observed X-ray emission. The 0.2–8.0 keV X-ray luminosity from the whole computational domain is (e.g., Silich et al. 2005)

$$L_x = 4\pi \int_{R_{\min}}^{R_{\max}} r^2 n_e n_i \Lambda_X(T, Z) dr, \qquad (4)$$

where the electron and ion number densities are $n_i = n_e = \rho/\mu_{\mathrm{ion}}$, μ_{ion} is the average mass per ion, $\Lambda_X(Z, T)$ is the X-ray emissivity (see Strickland & Stevens 2000), and $R_{\min}$ and $R_{\max}$ are the inner and outer boundaries of the computational domain, respectively. This is equal to about 2.5×10^{41} erg s^{-1} and 2×10^{42} erg s^{-1} for cases 2c and 2e, respectively. The luminosity of the infalling matter is even smaller. It is about 3.9×10^{40} erg s^{-1} and 1×10^{42} erg s^{-1} for cases 2c and 2e, respectively. This emission is orders of magnitude smaller than the SMBH luminosity, $L_{\mathrm{acc}} = \eta_{\mathrm{acc}} \dot{M}_{\mathrm{acc}} c^2$, where $\eta_{\mathrm{acc}} = 0.1$ is the accretion efficiency and c is the speed of light, which is $L_{\mathrm{acc}} \approx 8 \times 10^{44}$ erg s^{-1} in case 2c and $L_{\mathrm{acc}} \approx 8 \times 10^{45}$ erg s^{-1} in case 2e. And thus, it would be hard to quantify the infalling matter contribution to the total X-ray emission. In this case, low-luminosity AGNs (Terashima et al. 2002) seem to be better candidates to show the infalling matter X-ray emission, as in the case of the Seyfert 2/LINER galaxy NGC 4303. This shows the Raymond–Smith soft X-ray emission ($kT \approx 0.65$ keV) originating in the core of the galaxy with $r \leqslant 15$ pc, coincident with a young (age around 4 Myr, and a 3 pc radius), nuclear super star cluster (see Jiménez-Bailón et al. 2003).

4. THE STARBURST WIND AND THE SMBH ACCRETION RATE AND LUMINOSITY

The hydrodynamic solution discussed in the previous section allows one to calculate the accretion rate and thus the SMBH luminosity for each model presented in Table 1. The time-dependent accretion rates for models 2c–2f calculated as the mass flux through the inner grid boundary are shown as examples in Figure 5. At $t = 0$ Myr, the accretion rate, $\dot{M}_{\mathrm{acc}}$, is equal to zero because a stationary wind solution with $R_{\mathrm{st}} = 0$ was used as the initial condition (see Section 2.1). However, the accretion rate grows rapidly and reaches an average value of $0.14\ M_\odot$ yr^{-1}, $0.59\ M_\odot$ yr^{-1}, $1.36\ M_\odot$ yr^{-1}, and $2.38\ M_\odot$ yr^{-1} for models 2c–2f, respectively. Note that the accretion rate grows due to the larger stagnation volume and the larger mass deposition rate from more massive starbursts. After ~0.1 Myr, the total mass is conserved $\dot{M}_{\mathrm{NSB}} = \dot{M}_{\mathrm{acc}} + \dot{M}_w$; see Table 2 (Columns 3–5, respectively). Consequently, the fraction of the deposited mass expelled as superwinds from the starburst region decreases for more energetic starbursts although in absolute values it grows with the mass of the considered starburst (see Table 2).

The stationary accretion rates onto the SMBHs, $\dot{M}_{\mathrm{acc}}$, and the stationary rate at which matter is ejected as a starburst wind, $\dot{M}_w$, obtained through the numerical integration of the flow equations and normalized to the total mass deposition rate, $\dot{M}_{\mathrm{NSB}}$, are shown in Figure 6(a) as a function of the normalized starburst mechanical luminosity, $L_{\mathrm{NSB}}/L_{\mathrm{crit}}$. The circles represent the results from the numerical simulations of models 2a–2e. The solid and dashed lines present the semi-analytic $\dot{M}_{\mathrm{acc}}$ and $\dot{M}_w$, respectively. The mass accretion rate onto the SMBH grows more rapidly when the starburst mechanical power exceeds the
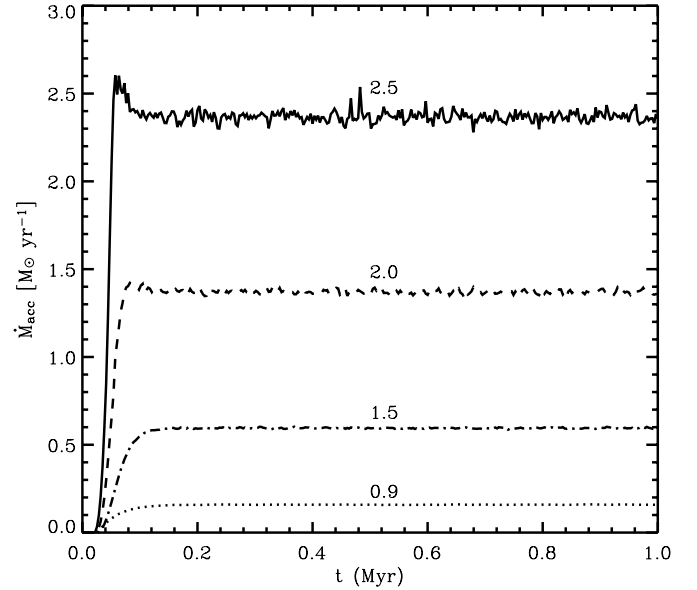
Figure 5. Time evolution of the mass accretion rate. The accretion rate onto the central $10^8\ M_\odot$ black hole for models 2c–2f; dotted, dash-dotted, dashed, and solid lines, respectively. The labels indicate the $L_{\mathrm{NSB}}/L_{\mathrm{crit}}$ values. Note that after ~0.1 Myr, $\dot{M}_{\mathrm{acc}}$ remains almost constant, and these values are reported in Table 2 together with $\dot{M}_{\mathrm{NSB}}$ and the resultant $\dot{M}_w$. Note also that the accretion rate associated with model 2f exceeds the Eddington limit. The small amplitude oscillations observed, mainly in models 2e and 2f, are numeric artifacts.

critical value ($L_{\mathrm{NSB}} > L_{\mathrm{crit}}$). This leads to a rapid increase in the central SMBH luminosity, $L_{\mathrm{acc}} = \eta_{\mathrm{acc}} \dot{M}_{\mathrm{acc}} c^2$, as shown in Figure 6(b). There, the open circles result from our numerical simulations, the solid and dotted lines present the semi-analytic results for starbursts with $R_{\mathrm{NSB}} = 10$ pc (models 2a–2e; see Table 1), and $R_{\mathrm{NSB}} = 40$ pc (models 1a–1d), respectively. The cross symbols mark the critical luminosity value ($L_{\mathrm{NSB}} = L_{\mathrm{crit}}$). Note that the accretion rate and the SMBH luminosity obtained numerically are in good agreement with those predicted by the semi-analytic model, even for starbursts with $L_{\mathrm{NSB}} > L_{\mathrm{crit}}$. This implies that the semi-analytic calculations lead to the correct value of the stagnation radius and thus may be used to estimate both the starburst wind power and the accretion onto the central SMBH and its corresponding luminosity, in all cases (above and below the threshold line).

Note that in both sets of calculations (R_{NSC} equal to 10 pc and 40 pc, with the assumed $V_{A,\infty} = 1500$ km s^{-1}) the accretion rate reaches values $\sim1.4\ M_\odot$ yr^{-1} when $L_{\mathrm{NSB}} \sim 2L_{\mathrm{crit}}$. This could result in $\sim50\%$ increase in the mass of the SMBH after ~50 Myr. Note also that the calculated accretion luminosity exceeds the Eddington limit (see Table 2, models 1e, 2f–2h) when the starburst mechanical luminosity is just about twice its critical luminosity. Certainly, the accretion rate and hence the SMBH luminosity could be reduced if additional physics are included in the model. For example, one could think of a 2D or 3D geometry that could account for the radiative and/or mechanical feedback from the central AGN and the redistribution of the net angular momentum in the accretion flow (e.g., Schartmann et al. 2009). However, our 1D model accounts for a realistic deposition of mass and energy around a central SMBH, and hence the results here presented give a good estimate of the accretion rate upper limit. And most important of all is that the model establishes a direct interplay between NSBs and their central SMBHs, in which all the reinserted matter unable to join the superwind becomes available to the SMBH.
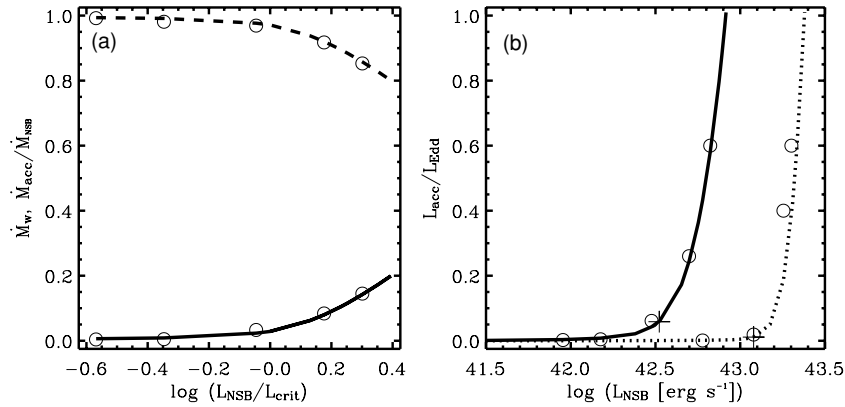
Figure 6. Semi-analytic and numerical predictions for the accretion rate and the SMBH luminosity. Panel (a) presents the calculated mass accretion rate and the rate at which mass is expelled as a superwind (circles) for starbursts below and above the threshold line (models 2a–2e). These are compared with the semi-analytic predictions (solid and dashed lines, respectively). All rates have been normalized to the total starburst mass deposition rate, $\dot{M}_{NSB}$. Panel (b) shows the SMBH luminosity normalized to the Eddington limit. The circles represent results from the numerical simulations; solid and dotted lines show semi-analytic calculations for starbursts with 10 pc (models 2a–2e) and 40 pc (models 1a–1d), respectively. An accretion efficiency of $\eta_{acc} = 0.1$ was used in the calculations. Cross symbols represent starbursts with the critical energy (L_{crit}) input rate.

The starburst wind, on the other hand, is sufficiently powerful in all cases as to significantly re-structure the host galaxy ISM, leading perhaps to a thick ring along the plane of the galaxy, and to a supergalactic wind along the host galaxy symmetry axis (as in Tenorio-Tagle & Muñoz-Tuñón 1997, 1998).

A simple estimate of the wind power can be obtained from its ram pressure (P_{ram}) at the starburst edge; see Column 7 in Table 2. This is, in all cases, many orders of magnitude larger than the typical ISM pressure in our Galaxy ($\sim 10^{-12}$ dyn cm^{-2}). It also exceeds by almost 3 orders of magnitude the pressure exerted by a one particle per cubic centimeter ISM, freely falling onto the starburst ($P_{ISM} = \rho_{ISM} v_{ff}^2$) with $v_{ff} = [2G(M_{BH} + M_{NSB})/R_{NSB}]^{1/2}$. The implication is thus that the resultant winds are to lead to the buildup of superbubbles and probably to supergalactic winds, preventing, in most cases, the falling of the ISM onto the NSB. Perhaps only an extremely dense ISM ($\rho_{ISM} \sim 10^{-20}$–10^{-21} g cm^{-3}) freely falling onto the central starburst would modify the structure of the outflow.

5. CONCLUSIONS

By means of 1D numerical simulations and semi-analytic estimates, we have worked out the stationary hydrodynamic solution for the matter reinserted by stellar winds and Type II SNe from a young, massive, and compact starburst in the presence of a central SMBH. The solution is bimodal in all cases, below and above the threshold line (L_{crit}), with a stagnation radius (R_{st}) which defines the outer boundary of the accretion flow onto the SMBH as well as the inner boundary of the starburst wind.

We have shown that at the stagnation radius, the force of gravity perfectly balances the outward pressure gradient acquired by the thermalized reinserted matter. We have also shown that radiative cooling becomes an important issue for massive starbursts with a mechanical luminosity above the threshold line ($L_{NSB} > L_{crit}$). In all these cases, radiative cooling depletes the pressure established through thermalization of the injected matter, and this leads to the development of a thermal instability in the accretion flow. The stagnation radius then moves rapidly toward the starburst boundary, with the mass of the considered starburst. In all simulations with $L_{NSB} > L_{crit}$, strong radiative cooling occurs at a radius interior to the stagnation radius. Radiative cooling re-structures the inner accretion flow, lowering

the temperature to the lowest allowed value, $T = T_{min}$. From then onward, and despite the continuous input of energy, the rapid velocity increase leading to a rapid density enhancement keeps and sustains the infalling gas temperature at $T = T_{min}$. It is the larger mass deposition rate, provided by more massive starbursts, that triggers the onset of strong radiative cooling and with it the shift of the stagnation radius toward the starburst boundary. This results in a rapid increase of the central SMBH luminosity for starbursts further above the critical threshold in the L_{NSB}–R_{NSB}–M_{BH} parameter space.

The larger mass deposition rates provided by more massive starbursts also lead to more powerful starburst winds, and an estimate of their mechanical power rules out the possibility of the ISM feeding the SMBH, at least during the Type II SN era.

Clearly, spherically symmetric calculations, such as the ones presented here, cannot account for the redistribution of the net angular momentum in the accretion flow. Nevertheless, they provide a good estimate of the upper limit to the accretion rate onto the central black hole, while pointing to a direct physical link between NSBs and the central SMBH luminosity. Our calculations do realistically account for the symmetric deposition of mass and energy from massive stars around the central object. This suggests that in a more realistic 2D or 3D geometry, able to account for the redistribution of the net angular momentum, the hydrodynamics would still lead to a bimodal solution with an accretion flow and an outward wind. In such a case, however, the residual angular momentum could favor the formation of a gaseous disk well contained within the NSB region. We shall consider some of these issues in a future communication.

REFERENCES

Alexander, D. M., Bauer, F. E., Chapman, S. C., Smail, I., Blain, A. W., Brandt, W. N., & Ivison, R. J. 2005, ApJ, 632, 736

Begelman, M. C., & Nath, B. B. 2005, MNRAS, 361, 1387

Booth, C. M., & Schaye, J. 2009, MNRAS, 398, 53

Chen, Y. M., Wang, J. M., Yan, C. Y., Hu, C., & Zhang, S. 2009, ApJ, 695, L130

Cid Fernandes, R., & Terlevich, R. 1995, MNRAS, 272, 423

Ciotti, L., & Ostriker, J. P. 2001, ApJ, 551, 131

Ciotti, L., Ostriker, J. P., & Proga, D. 2009, ApJ, 699, 89

Clarke, C. J., & Carswell, R. F. 2007, Principles of Astrophysical Fluid Dynamics (Cambridge: Cambridge Univ. Press)

Côté, P., et al. 2006, ApJS, 165, 57

Davies, R. I., Mueller Sánchez, F., Genzel, R., Tacconi, L. J., Hicks, E. K. S., & Friedrich, S. 2007, ApJ, 671, 1388

Di Matteo, T., et al. 2005, Nature, 433, 604

González-Delgado, R. M., Cid Fernandes, R., Pérez, E., Martins, L. P., Storchi-Bergmann, T., Schmitt, H., Heckman, T., & Leitherer, C. 2004, ApJ, 605, 127

Hao, C. N., Xia, X. Y., Mao, S, D., Deng, Z. G., & Wu, H. 2008, Chin. J. Astron. Astrophys., 8, 12

Hao, C. N., Xia, X. Y., Mao, S., Wu, H., & Deng, Z. G. 2005, ApJ, 625, 78

Heckman, T. M. 2009, in Astrophysics in the Next Decade, Astrophysics & Space Science Proceedings, ed. H. A. Thronson, M. Stivelli, & A. Tiellens (Dordrecht: Springer), 335

Imanishi, M. 2003, ApJ, 599, 918

Jiménez-Bailón, E., Santos-Lleó, M., Mas-Hesse, J. M., Guainazzi, M., Colina, L., Cerviño, & González-Delgado, R. 2003, ApJ, 593, 127

Leitherer, C., et al. 1999, ApJS, 123, 3

Lípari, S. L., & Terlevich, R. J. 2006, MNRAS, 368, 1001

Nulsen, P. E. J., & Fabian, A. C. 2000, MNRAS, 311, 346

Plewa, T. 1995, MNRAS, 275, 143

Rossa, J., van der Marel, R. P., Böker, T., Gersen, J., Ho, L. C., Rix, H.-W., Shields, J. C., & Walcher, C.-J. 2006, AJ, 132, 1074

Schartmann, M., Meisenheimer, K., Klahr, H., Camenzind, M., Wolf, S., & Henning, Th. 2009, MNRAS, 393, 759

Seth, A., Agüeros, M., Lee, D., & Basu-Zych, A. 2008, ApJ, 678, 116

Silich, S., Tenorio-Tagle, G., & Añorve Zeferino, G. A. 2005, ApJ, 635, 1116

Silich, S., Tenorio-Tagle, G., & Hueyotl-Zahuantitla, F. 2008, ApJ, 686, 172

Silich, S., Tenorio-Tagle, G., & Rodríguez González, A. 2004, ApJ, 610, 226

Silk, J., & Rees, M. J. 1998, A&A, 331, L1

Somerville, R. S., Hopkins, P. F., Cox, T. J., Robertson, B. E., & Hernquist, L. 2008, MNRAS, 391, 481

Stone, J. M., & Norman, M. L. 1992, ApJS, 80, 753

Strickland, D. K., & Stevens, I. R. 2000, MNRAS, 314, 511

Tenorio-Tagle, G., & Muñoz-Tuñón, C. 1997, ApJ, 478, 134

Tenorio-Tagle, G., & Muñoz-Tuñón, C. 1998, MNRAS, 293, 299

Tenorio-Tagle, G., Wünsch, R., Silich, S., & Palouš, J. 2007, ApJ, 658, 1196

Terashima, Y., Iyomoto, N., Ho, L. C., & Ptak, A. 2002, ApJS, 139, 1

Veilleux, S., Cecil, G., & Bland-Hawthorn, J. 2005, ARA&A, 43, 769

Wada, K., & Norman, C. A. 2002, ApJ, 566, L21

Wada, K., Papadopolous, P. P., & Spaans, M. 2009, ApJ, 702, 63

Walter, F., Riechers, D., Cox, P., Neri, R., Carilli, C., Bertoldi, F., Weiss, A., & Maiolino, R. 2009, Nature, 457, 699

Watabe, Y., Kawakatu, N., & Imanishi, M. 2008, ApJ, 677, 895

Wehner, E. H., & Harris, W. E. 2006, ApJ, 644, L17

Wünsch, R., Tenorio-Tagle, G., Palouš, J., & Silich, S. 2008, ApJ, 683, 683